Available online at www.sciencedirect.com

ScienceDirect

Advances in Space Research xxx (xxxx) xxx

ADVANCES IN SPACE RESEARCH (a COSPAR publication)

www.elsevier.com/locate/asr

Quantitative analysis of spatial distribution of land surface temperature (LST) in relation Ecohydrological, terrain and socio- economic factors based on Landsat data in mountainous area

Farideh Taripanah *, Abolfazl Ranjbar

Department of Desert Control and Management, University of Kashan, Iran

Received 5 December 2020; received in revised form 29 June 2021; accepted 6 July 2021

Abstract

Land surface temperature (LST) is considered as one of the most significantly effective factors on the regional climate and ecology, playing an important role in connecting surface energy and water exchange. In mountainous regions, LST reveals lots of inconsistencies due to the effect of such factors as topography, vegetation, solar radiation, etc. We sought to investigate the the temporal and spatial variation LST in different years and its relationship with effective factors in 5 dimensions using Multiple statistical methods, the sepidan region in northwest Iran. The multi-factorial land use, topographic (elevation, slope, aspect), biophysical indices (normalized difference vegetation index (NDVI), normalized difference moisture index (NDMI), normalized difference built up index (NDBI), and modified of normalized difference water index (MNDWI)), socio-economic (fossil fuel CO_2 emissions (FFCOE) and road density(RD)), and climate (temperature and solar radiation) was studied in the current research. To this end, Images of July 1998 and 2017 were extracted from Thematic Mapper (TM5) and Operational Land Imager/Thermal infrared sensors (OLI/TIRS8). Moreover, ordinary least squares regression (OLS), Best subset regression, and Hierarchical Partitioning Analysis (HP) were used to investigate the relationship between LST and relevant effective factors. The results indicated that the temperature range varied from 10 to 53 °C in the time period mentioned. The highest amount of LST was observed in barren land use and the lowest one was found in garden lands. An negative correlation was found between LST and elevation. On the other hand, the highest value of the Laps rate of surface temperature was observed in the southern aspects and the lowest one was observed in the western aspects. Furthermore, the highest and lowest values of lase rate were found in slopes less than 10°, and in 50 to 60-degree slopes, respectively. The results of the OLS correlation indicated a negative correlation between LST and NDVI, NDMI, and MNDWI, and a positive correlation of LST with climatic and socio-economic indicators. LST's highest and lowest correlations were found to be with vegetation ($R^2 = 0.95$) and road density ($R^2 = 0.1$). Finally, while in 1998 temperature and vegetation were identified as the most influential factors on LST, it was the elevation that was found to be the most effective factor on LST in 2017 with the effective rate of 82.72%. This study offers a valuable viewpoint on the temporal and spatial variations of LST, their complexity, and the environmental factors that affect them. The viewpoint could, therefore, be used for prospective studies on the analysis of the ecosystem's reaction to climate changes.

Keywords: Land surface temperature (LST); Driving factors; Ordinary least squares regression (OLS); Best subset regression; Hierarchical cluster analysis; Iran

1. Introduction

Mountainous regions play an important and effective role in the global energy balance and the formation and

* Corresponding author.
E-mail addresses: Taripanah.f@gmail.com (F. Taripanah), aranjbar@kashanu.ac.ir (A. Ranjbar).

https://doi.org/10.1016/j.asr.2021.07.008
0273-1177/© 2021 Published by Elsevier B.V. on behalf of COSPAR.

evolution of the climate (Van De Kerchove et al., 2013). Moreover, as the temporal and spatial distribution increases, surface temperature and water expand the geographical latitude of the climate (Aguilar et al., 2010; Ivanov et al., 2008). Mountainous ecosystems are, therefore, vulnerable regions that are more sensitive than the plains to the natural and humane factors (Shi et al., 2019). Thus, the analysis of near-surface processes is considered an essential part of environmental researches carried out on mountainous regions (He et al., 2018). Surface temperature is regarded as a significant factor in controlling the exchange of energy at the surface of the earth, being used for studying the physical properties of surface processes and climate change (Li et al., 2013; Berg et al., 2014; Tomlinson et al., 2011).

Temporal and spatial changes of land surface temperature (LST) has, generally, been investigated in many environmental studies such as those carried out on surface energy management, surface water cycle, vegetation management, and environmental and urban climate assessment (Xu et al., 2016; Holzman et al., 2014; Zhou et al., 2013; Amiri et al., 2009). LST is affected at different scales by a variety of factors including the topographic conditions, energy levels, climatic conditions, land use, vegetation, and geographical location (Gluch et al., 2006; Peng et al., 2018). Terrestrial meteorological data (Eludoyin et al., 2013) and remote sensing are two methods which are used for investigating LST (Li et al., 2013; Peng et al., 2012). However, on large temporal and spatial scales, terrestrial measurement is difficult to conduct due to its high costs and time-consuming nature. Moreover, in difficult to reach terrains such as mountains, scattered and irregular distribution, as well as the insufficient number of meteorological stations, may challenge and limit the accuracy and applicability of the traditional method (Steinacker et al., 2006; Neteler, 2010). On the other hand, remote sensing data have been used by many researchers to study the components of energy balance such as albedo and LST because of their ease of access, high resolution, and suitable spatial coverage (Ayansina, 2016; Clinton and Gong, 2013; Mihalcea et al., 2008). From among different sets of satellite images, ASTER /EOS-TERRA (Advanced Spaceborne Thermal Emission and Reflection Radiometer) and sensors of Landsat series (TM Band 6 (120 m) ETM(Enhanced Thematic Mapper Plus) Band6 (60 m) and OLI/TIRS B10(100 m)) display the LST with 60–120 spatial resolution (Estoque et al., 2017; Kikon et al., 2016; Sattari et al., 2018). while the same data could be accessed daily through other sensors such as MODIS and AHVRR with a low spatial resolution (1000 m) (Meng et al., 2018; Yao et al., 2018; Yue et al., 2019; Zhou et al., 2018).

In mountainous regions, the temporal and spatial distribution of LST is affected by different meteorological, topographic factors as well as vegetation and soil (Li et al., 2014). The factors affecting LST could generally be classified into four categories: 1) topography, 2) surface biophysical parameters, 3) socio-economic and 4) climatic (Minder et al., 2010; Peng et al., 2018; Chang et al., 2017). The relationship between LST and elevation would fundamentally be modified under the influence of local topography. It would also change with the effect of slope and aspect. Differences in aspect play such an important role in controlling the temperature that solar radiation is lower in northern hills than the southern ones (McCutchan and Fox, 1986).

Due to the richness of land use and land cover information, surface biophysical parameters have been widely used in LST correlation analysis. The normalized difference vegetation index (NDVI), normalized difference moisture index (NDMI), normalized difference built up index (NDBI), and modified of normalized difference water index (MNDWI) indicating a significant correlation with LST (Lu et al., 2013) and the population growth considerably affect heat islands (Kotharkar and Surawar, 2016; Huang et al., 2016). Most of the researches carried out in this regard have studied only one factor and other effective socio-economic factors on LST such as road density, fossil fuel, night light, etc. have remained under-researched. From among climatic factors, the air temperature has the strongest correlation with LST, but the two factors differ in value, measurement method, and response to weather conditions (Jin and Dickinson, 2010). Few studies have already been done on the influence of different factors especially air temperature and solar radiation on LST. For instance, He et al. (2019) studied the effect of terrestrial factors on LST in Chinese mountainous Regions. The results of their study indicated a reverse correlation of LST with elevation and solar radiation angle. They also found that changes of LST were greater in southern aspects than the other ones, with the vegetation being a key factor in the extent of LST changes. Alemu (2019) investigated the temporal and spatial changes of LST concerning NDVI in the watershed and showed that there was an negative correlation between surface temperature and NDVI. Having studied the relationship between LST, land use, and geological formation, Ibrahim and Abu-Mallouh (2018) reported that the highest surface temperature had been observed in rocky lands and basaltic formations, which was due to the nature of those formations. Chen and Zhang (2017) proved an negative correlation between LST and MNDWI, and a positive correlation between LST and NDBI. Dissanayake et al. (2019) showed a positive correlation between fossil fuels and population density in terms of socio-economic factors.

In general, most of the studies carried out on the effects of land cover changes on LST have focused on the description of LST's spatial characteristics. Although the findings of these studies are important, they rarely discuss the relationship between LST and different factors. Climatic conditions and local factors including DEM, slope, aspect, solar altitude angle, the type of solar material, soil moisture, and humidity are highly effective on LST. Compared with the

possible effect of only a single factor on LST, the earth's surface temperature is highly affected by changes in multiple factors.

The possible effects of various factors such as MNDWI, NDBI, NDVI, NDMI, slope, aspect, elevation, land use, air temperature, solar radiation, etc. on LST and the way they affect it have received less attention. Lack of sufficient researches on the relationship between LST and different factors prevents offering more effective managerial solutions to reduce LST. Furthermore, while most of the studies carried out in this regard have used stepwise regression as their statistical method, the current study used Best-subset and Hierarchical partitioning analysis to identify the most effective factors on LST. To this end, the Sepidan region in Fars province, Iran, was selected as a case to be studied in that regard.

This study set out to identify the factors which affect LST, using linear regression in a mountainous region. Specifically, the main goals of the study were as follows: 1) investigating the temporal and spatial distribution of LST for the 1998–2017 period; 2) using ordinary least squares regression for determining the relationship between LST and different factors; 3) using best –Subset regression to identify the best applicable model in this regard, and Hierarchical partitioning to detect the main effective factors on LST.

2. Materials and method

2.1. he study region

Thee Sepidan county is, with an area of 290000 ha, located in the northern part of Fars province, Iran. It occupies 2.3 percent of the Fars province and is located at 52° 40′ East latitude and 30° 35′ North longitude. It is a mountainous region covered with jungle whose altitude from the sea surface is estimated as 2225 m (Fig. 1) As for its high annual precipitation, the region is characterized by snowy winters and watery summers. As environmentally valuable assets, the jungles located at Sepidan county and Zagros area are protected zones. Being located in central Zagros, the county has cold snowy winters and moderate summers. The average annual precipitation and temperature rates of the region are 518 mm and 15 °C respectively. Moreover, its average minimum and maximum temperature are 9.2 °C and 19 °C respectively. In general, the climate of the county varies from semi-arid in its eastern part to very humid in its northwest (Esfandyari Bayat and Rameh, 2016).

2.2. Dataset

To examine LST, this study used cloud-free multi-time images of Landsat with their Row and Path being 163 and 39 respectively, which were downloaded from the following dataset: https://earthexplorer.usgs.gov. The selected images had been taken in May to September 1998 and 2017 by Landsat 5 and 8, along with TM and OLI/TIRS sensors (Table 1). Having downloaded the satellite images, radiance calibration and atmospheric correction were performed on them at the pre-processing phase in ENVI 5.3 software to eliminate the errors caused by the sensor and atmosphere. As the vegetation of the study area (native and domestic) reveals the highest annual vital activity from May to September, NDVI values of such a period were used to evaluate the vegetation (Jin et al., 2009). Digital elevation model (DEM) with a resolution of 30 m was extracted from https://gdex.cr.usgs.gov/gdex. Climatic indices used in the present study included the average annual temperature and solar radiation whose meteorological data were collected on a monthly basis for the study period from 17 local meteorological stations. The data regarding road density were collected from Open Street Map website (http://www.openstreetmap.org). To estimate the road density, then, the data were analyzed via ArcGIS10.3 software. The fossil fuel CO2 emission data set was obtained from open-data inventory for anthropogenic carbon dioxide (ODIAC) which has been produced by the World Environmental Research Center, National Institute of Environmental Studies and is available from http://db.cger.nies.go.jp/dataset/ODIAC/ emission_dataset.html (Table 2).

2.3. Methods

2.3.1. Calculating the land surface temperature (LST)

The map of the land surface temperature was drawn based on the Landsat data, using Digital Numbering and Thermal Bands (Band 6 in TM Landsat, and Band 10 in OLI/TIRS Landsat). To this end, the spectral radiance of($SpectralRadiances; L\lambda$)Multispectral and thermal Bands of Landsat images would be calculated in the first phase via equations (1) and (2). In the second phase, the spectral radiance would be transformed into Brightness Temperature through the constants presented in the reference file. Here, the brightness Temperature is calculated via equation (3) (Nurwanda and Honjo, 2018):

$$L\lambda(Landsat5TM\ \ and\ \ 7\ \ ETM) = Lmin + \left(\frac{Lmax - Lmin}{255}\right) \times DN \tag{1}$$

$$L\lambda(Landsat8\mathrm{OLI/TIRS}) = ML \times DN + AL \tag{2}$$

$$TB = \frac{K2}{\ln\left\lfloor\left(\frac{K1}{L\lambda}\right) + 1\right\rfloor} - 273.15 \tag{3}$$

where L_{max} and L_{min} are available in the satellite header file (metadata). ML stands for Band specific multiplicative rescaling (0.0003342), AL stands for Band specific additive rescaling (0.1), K1 stands for first thermal constant and K2 stands for second thermal constant (in Landsat TM5: K1 = 607.76 and K2 = 1260.56, and in Landsat 8TIRS, K1 = 774.8853 and K2 = 1321.0789 for band10,

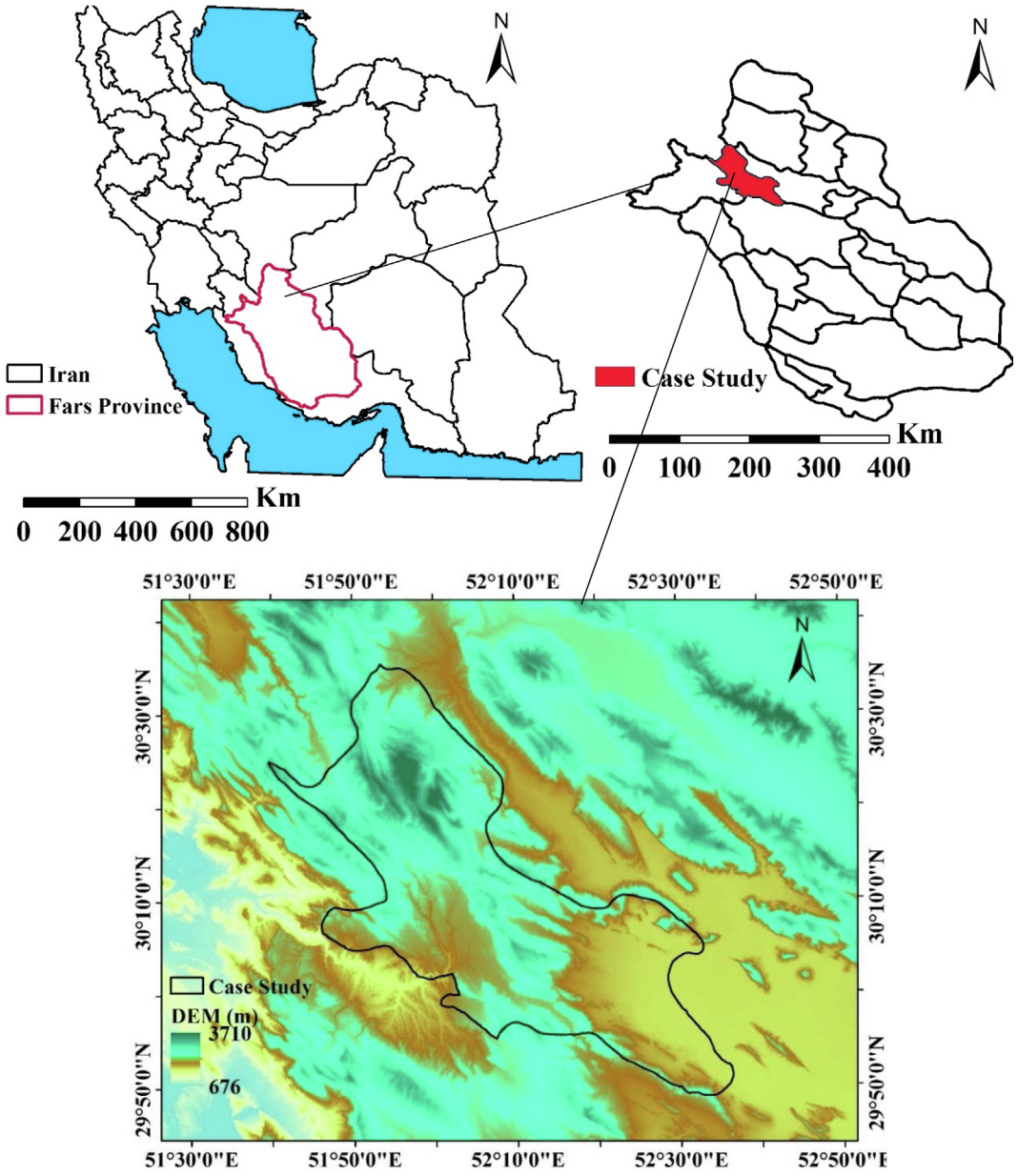

Fig. 1. Geographical Location of the study area in southwestern Iran, Black lines boundary field.

Table 1
Dataset obtained from United States Geological Survey (USGS) for the present study.

No.	Sensor	Acquisition Year	Acquisition Date	Acquisition Time(GTM)
1	Landsat 5 TM	1998	1998–06-12	06:41:09
2			1998–06-28	06:41:19
3			1998–07-14	06:41:38
4			1998–07-30	06:41:32
5			1998–08-15	06:41:56
6			1998–08-31	06:41:56
7			1998–09-16	06:42:04
8	Landsat 8OLI/TIRS	2017	2017–06-16	07:02:57
9			2017–07-02	07:03:06
10			2017–07-18	07:03:02
11			2017–08-03	07:03:13
12			2017–08-19	07:03:19
13			2017–09-04	07:03:21
14			2017–09-20	07:03:24

Table 2
Type of data used in the study.

Type of data	Description	Source
Landsat Imageries	Biophysical indeces (NDVI, NDMI, NDBI, MNDWI) and LST	United States Geological Survey (USGS): https://earthexplorer.usgs.gov
DEM	Terrain Factors (elevation, aspect, slope)	https://gdex.cr.usgs.gov/gdex
Meteorological Data	Climatic indices (Temperature, Solar radiation)	Iran Meteorological Organization
Scio – economic data	FFOCE, RD	World Environmental Research Center, National Institute of Environmental Studies: http://db.cger.nies.go.jp/dataset/ODIAC/ emission_dataset.html, Open Street Map website: (http://www.openstreetmap.org)

K1 = 480.88 and K = 1201.14 for band 11) (32). In the third phase, NDVI was calculated through equation (7) and, then, Fractional Vegetation cover (FVC) was calculated via equation (4) (Sobrino et al., 2004):

$$\mathrm{FVC} = \left(\frac{\mathrm{NDVI} - \mathrm{NDVImin}}{\mathrm{NDVImax} - \mathrm{NDVImin}}\right)^2 \quad (4)$$

In this study we used equation (5) to obtain emissivity values (Valor and Caselles, 2005):

$$\varepsilon = \varepsilon_V + \varepsilon_S(1 - \mathrm{FVC})(1 - 1.74\mathrm{FVC}) + 1.7374FVC(1 - FVC) \quad (5)$$

in equation (5),ε stands is Emissivity $\varepsilon_V$and $\varepsilon_S$are the emissivity assigned to full vegetation cover (0.985), and bare soil (0.960) respectively. Finally, the Land surface temperature was estimated through equation (6) (Sobrino et al., 2016):

$$LST = T_i + C_1(T_i - T_j) + C2\ (T_i - T_j)^2 + C0 + (C_3 + C_4w)(1 + \varepsilon\ ) + (C\ +\ Cw)\Delta\varepsilon \quad (6)$$

In this equation, LST stands for the land surface temperature based on °C, Ti and Tj are the Landsat 8 brightness temperatures of the two TIR bands (in °C), respectively; W is the atmospheric water vapor content (g.cm^2); ε and Δε stands are the mean and difference Emissivity which coulds be calculated through 0.5 ($\varepsilon_i + \varepsilon_j$) and ($\varepsilon_i - \varepsilon_j$), respectively. Finally Co to C6 are the coefficients of the equation, which obtained from the simulated data (C_0, -0.268 ± 0.014; C_1, 1.084 ± 0.010; C_2, 0.2771 ± 0.0017; C_3, 45.1 ± 0.7; C_4, -0.73 ± 0.19; C_5, -125.0 ± 1.7; C_6, 16.7 ± 0.5) (Sobrino et al., 1996)

2.3.2. Effective factors on LST

Biophysical factors are among the effective factors on LST which are taken into account in relevant studies. These factors are extracted through remote sensing and contain a lot of spectral information. As the most significant vegetation index, NDVI is used to indicate the coverage or status of vegetation. The values of this index vary from −1 to +1 (Rouse et al., 1974). In this study, NDMI was used to show the moisture of the soil surface. The values of this index vary from −1 to +1, with the higher values indicating areas with higher moisture levels such as water areas or areas covered by vegetation, and the negative values suggesting areas with lower moisture levels like the bare soil and buildings (Xu, 2005). MNDWI is made from a combination of green and mid-infrared bands. The green band (0.6–0.52 μm) is sensitive to differences in water turbidity, sediment, and pollution mass, while the mid-infrared band represents (1.6–1.7 μm) a stark contrast between soil and water properties with regard to the high degree of water absorption and the strong ground reflection; Therefore, the MNDWI algorithm is ideal for land–water discrimination (Ghosh et al., 2015). NDBI is used for identifying urban areas, the values of which are negative for areas covered by vegetation, and positive for urban areas (Liu and Zhang, 2011). Table 3 shows different methods for measuring these indices.

2.3.3. Preparing land-use maps

The present study considered six land-uses including residential area, rangeland, rain-fed farm, irrigated farm, orchard, and barren area were considered to study the trend of land-use changes. This study used the supervised classification method for preparing the land-use map. The topographies in the satellite imagery were detected by false color composite methods of FCC432 and FCC543 along with the contrast stretching. To better identity the surface features, the intended images were detected via color combination, contrast expansion, and band ratio. Having detected the images, they were classified via a maximum likelihood algorithm, using the supervised classification method. To evaluate the accuracy of the classification, the land-use maps supplied by the Office of Natural Resources and Google Earth were used to develop actual samples randomly taken from the region for each land-use/land-cover class. They were then implemented on the image and a classification error matrix was derived. This algorithm acts more accurately than other classification methods. In this matrix, statistical specifications are displayed for each class including producer's accuracy, consumer's accuracy, overall accuracy, and the kappa coefficient. This is one of the most well-known Kappa estimates made with the use of error matrix elements based on equation (7).

$$K = \frac{N\sum_{i=1}^{r} X_{ii} - \sum_{i=1}^{r} X_{i+}X_{+i}}{N^2 - \sum_{i=1}^{r} X_{i+}X_{+i}} \quad (7)$$

Table 3
Calculation of the biophysical indices used in the study.

Surface Biophysical index	Equation	
Normalized difference vegetation index(NDVI)	$NDVI = \frac{NIR-Red}{NIR+Red}$	Rouse et al., 1974
Normalized difference moisture index (NDMI)	$NDMI = \frac{NIR-MIR}{NIR+MIR}$	Xu, 2005
Modification of Normalized Difference Water Index (MNDWI)	$MNDWI = \frac{Green-MIR}{Green+MIR}$	Ghosh et al., 2015
Normalized difference built up index (NDBI)	$NDBI = \frac{MIR-NIR}{MIR+NIR}$	Liu and Zhang, 2011

In this equation, N stands for total pixels of observations, X_{i+} represents the sum of i-th row elements, and X_{+i} shows the sum of j-th column elements. The values of the Kappa coefficient vary between 0 and 1, with zero indicating a random and criteria-free classification while 1 suggesting a completely true classification based on the collected samples (Peng et al., 2017).

Table 4 shows all factors considered in this study within 6 categories including terrain factors (topography), land-use, green Space, humidity, climatic, and socio-economic. As for topographic factors, elevation, slope, and aspect were taken into account. The Land-use factor was used for landscape and NDVI was applied on green Space. In this study, NDMI and MNDWI were the moisture indices, and the socio-economic factors included road density (RD) and fossil fuel-based CO2 emissions (FFCOE). As for climatic factors, air temperature and solar radiation were taken into account. Moreover, 3000 points were randomly selected to be investigated in the study, and all the required analyses were carried out via SPSS24, ArcGIS 10.3, and Sigma plot 14.

2.3.4. Statistical methods used for the analysis of the findings

In this study, LST and 12 effective factors were determined for all selected points. First, the correlation between all variables was discovered, using Pearson correlation at a significance level of 5%. Then, LST was selected as the dependent variable and its relationship with all the 12 factors was identified via OLS regression to evaluate the effect of each of these factors separately.

In the second phase of the study, an optimal regression model was to be devised. Most of the studies carried out in this regard use stepwise regression to devise a regression model. However, as this type of regression introduces all effective factors separately in terms of their degree of importance, it cannot present all possible combinations (Krall et al., 1975). To resolve this problem, the current study used Best Subset regression which is a reliable model and considers the mixed effects of all possible factors and offers more information regarding their properties (Anthony and Kuk, 1984). SigmaPlot 14 software was used to devise this regression model and all possible models. The optimal regression model was then selected based on the R^2 index and Akaike information criterion (AIC).

Finally, hierarchical partitioning (HP) analysis was used to determine the independent influence of each effective factor in the optimal model. As this analysis determines the relative importance of each factor by overcoming the multi-linear process that is common in environmental variables, it could be considered as a suitable method in multi-dimensional environmental studies (Mac, 2000).

Table 4
Factors involved in Land Surface temperature in this study.

Categories of variables	variables
Terrain factor	Elevation
	Slope
	Aspect
Green space	NDVI
Water space	NDMI
	MNDWI
Impervious space	NDBI
Landscape	Land use/Landcover
Socio-economy	FFCOE
	RD
Climate	Air temperature
	Solar radiation

3. Results

3.1. Temporal and spatial distribution of land surface temperature

Fig. 2 shows the spatial distribution of LST in the Sepidan region in 1998 and 2017. While in 1998 LST varied from 11.28 °C to 48.52 °C with its average being 36.27 °C, in 2017 its numerical range varied from 17.60 °C to 51.58 °C with an average of 37.68 °C. In terms of spatial distribution within the time period studied, the highest value of LST was observed in the southern and southeastern parts, while the lowest value was observed in the northern, northwestern, small parts of the center and southeast. Thermal zoning was created for both periods through the natural break method and 6 temperature zones were obtained accordingly. In this regard, the LST of all the 6 zones mentioned was lower in 1998 than those found in 2017. The largest number of pixels in both periods was observed in LST 35 to 42 °C. On the other hand, the lowest number of pixels was found in the initial and final range.

3.2. Driving factors on LST

3.2.1. land-use

The results showed that the accuracy for both study periods was more than 95%, and the highest accuracy level was found in 2017 with 99.9% (Table 5). The kappa coefficient was also more than 85% for both periods, with its

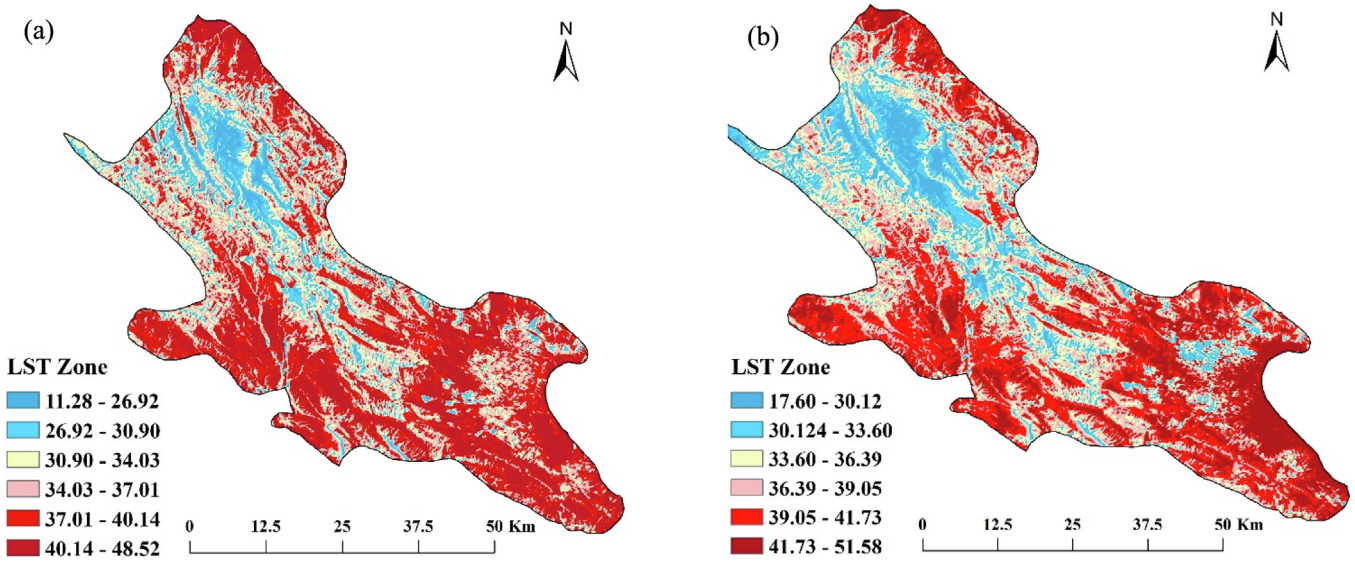

Fig. 2. LST zone maps in July 1998 (a) and July 2017 (b).

highest value found in 2017 at 96.4%, proving high accuracy of the classification which is, thus, consistent with the results found by Nurwanda and Honjo (2018).

Fig. 3a,b, shows the classification map of land-use for the 1998–2017 study period. The details of the total area and the proportion of each use are shown in Fig. 3c. The results generally indicate some changes in the area of different types of land-use in 2017 compared with those found in 1998, with farmlands, gardens, residential areas, and bare soil-filled areas experiencing approximately -%21, +% 14.42, + %1.54, and +%1.89 changes respectively in 2017 in comparison with 1998.

The lowest LST values in 1998 and 2017 were 30 and 36, respectively, which was different from the temperature values in the whole study area and was observed in garden use, whereas the highest LST values in 1998 and 2017 were found, respectively, in bare soil and residential lands (Fig. 3d).

Fig. 4 shows the percentage of land-use in different LST classes within the study period. In 1998, the highest percentage of vegetation which belonged to the Irritated farm and garden was observed in class 1, whereas in 2017 vegetation of irrigated farm and garden decreased and that of the residential areas increased. Compared with 1998, the percentage of LST classes in residential areas increased in 2017.

3.2.2. Topographic factors

The effect of elevation on LST is shown in Fig. 5. The effect of elevation on LST was similar to its effect on air temperature. Elevation had a significant correlation with LST at the 0.01 and 0.05 level. An negative correlation was found between these two factors in the study area. Moreover, the coefficient of determination (R^2) was higher in 2017 than in 1998. In 1998 and 2017, R^2 levels were determined as 0.54 and 0.15, respectively. Furthermore, RSME was calculated as 3.55 for these two periods. Finally, the regression analysis of these two factors indicated that LST decreased with the increase of elevation.

Slope and aspect are two effective factors on LST in sunny and shaded hills. The lapse rate of land surface temperature was investigated in 9 different aspects. The laps rate value was higher in 2017 than in 1998. According to Fig. 6a, the lapse rate was more than 16 °C in different aspects throughout the study period. The maximum value of the lapse rate was observed in the flat and southeast aspects and its minimum value was found in the western aspect.

The slope factor controls the level of incoming radiation through the angle between the earth's slope and solar radiation. That is why the incoming solar radiation on the surface of the earth is sensitive to the slope and influences the surface temperature. In this study, therefore, the slope was classified into 10̊ classes where laps rate was investigated (Fig. 6b). According to the results of this part, the highest value of lapse rate for the 1998–2017 period was observed in slopes less than 10°, and its lowest value was found in slopes with more than 50°. Generally, the results indicated a decreasing trend of the LST's lapse rate with an increase in slope.

Table 5
Assessing the overall accuracy and kappa coefficient of different types of land use.

Overall accuracy(%)	kappa coefficient	Year
98.3	0.8881	1998
99.9	0.964	2017

3.2.3. Biophysical index

Fig. 7a,b shows the distribution of NDVI for 1998 and 2017. While the NDVI values varied from −0.35 to 0.76 for the 1998 period, they ranged between −0.36 to 0.82 in 2017. The increase in NDVI in 2017 could be attributed to the increase in vegetation in the agricultural sector. With

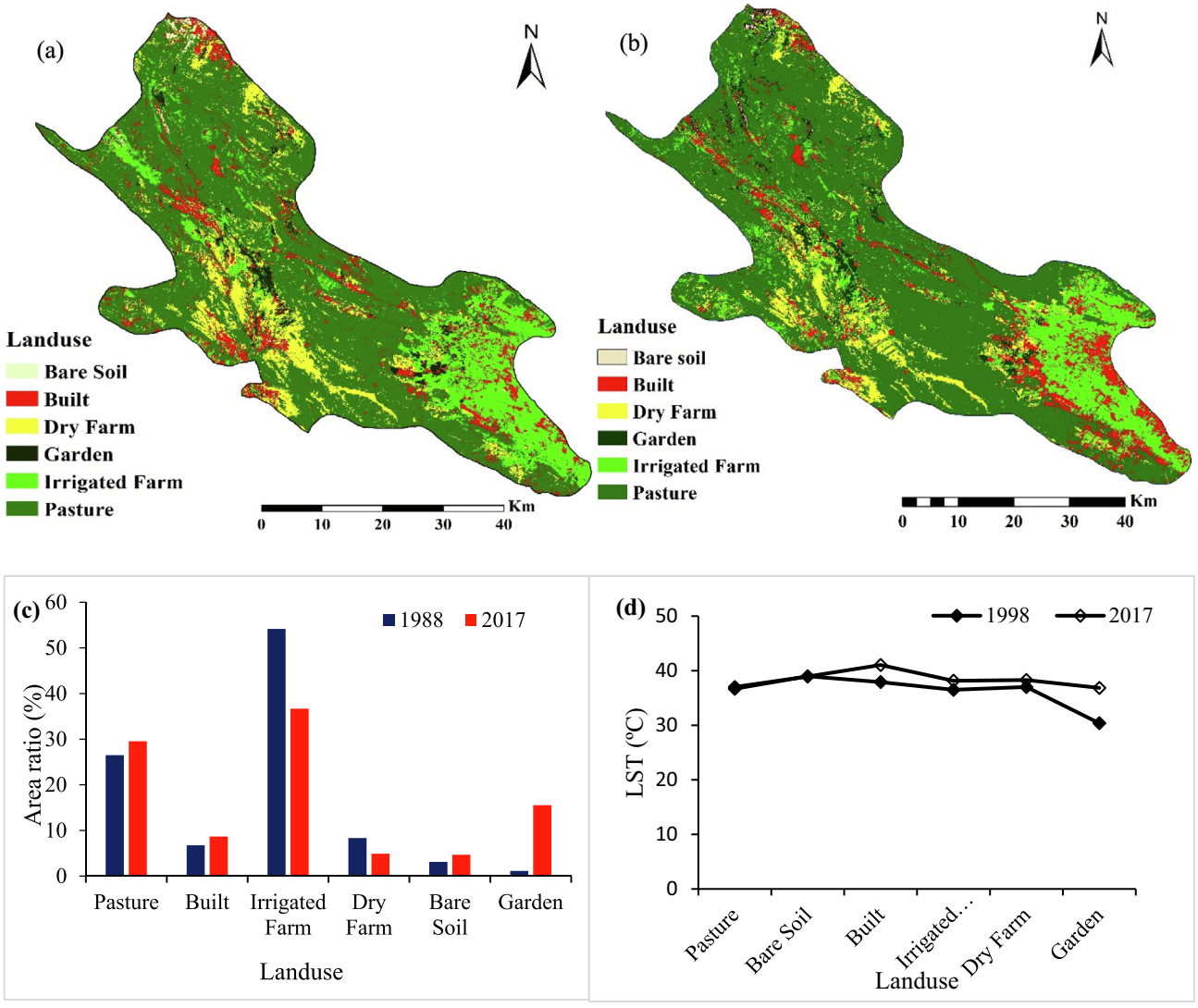

Fig. 3. Land use maps in July 1998 (a), July 2017 (b) Various land use areas in (c) and LST values in different land-use 1998–2017 period.

an increase in surface vegetation, a decreasing trend was observed in LST, indicating the direct effect of vegetation on controlling the evaporation, thermal properties, and surface radiation balance. The R^2 value between NDVI and LST was greater in 2017 (0.41) than in 1998 (Table 6). LST changes ranged from 10 to 40 °C in 1998, but in 2017

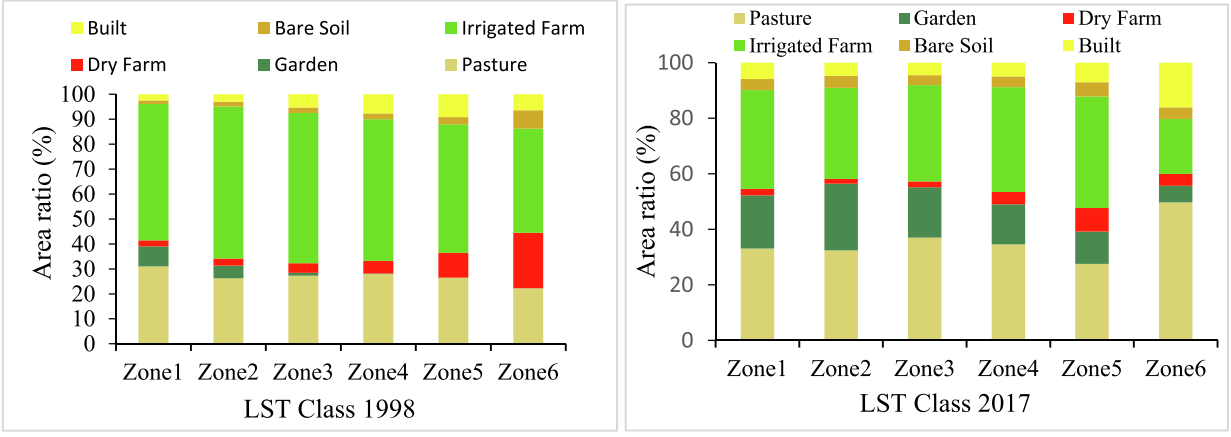

Fig. 4. The distribution of different land uses in various LST zones.

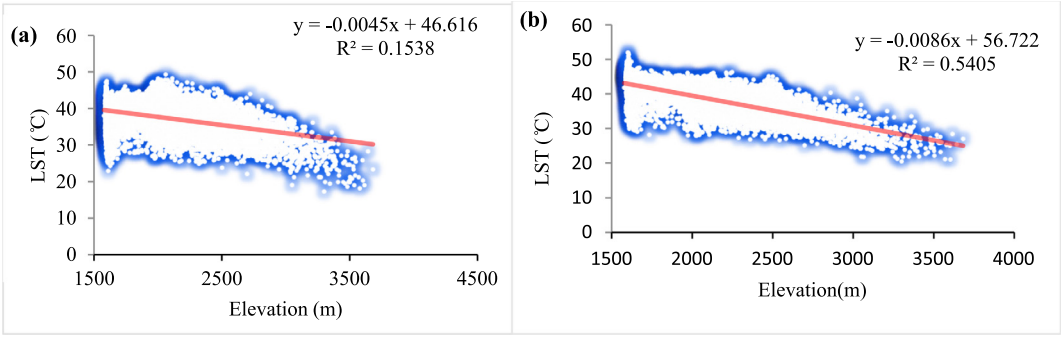

Fig. 5. The scatter plot between elevation and LST in the study area from 1998 to 2017.

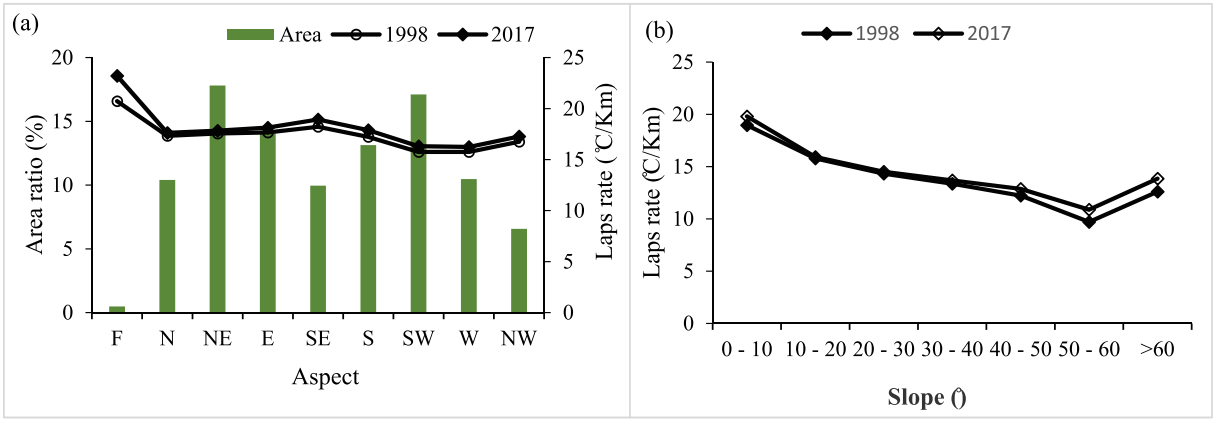

Fig. 6. Variability in the lapse rates of the study area at different aspect (a) and slope (b).

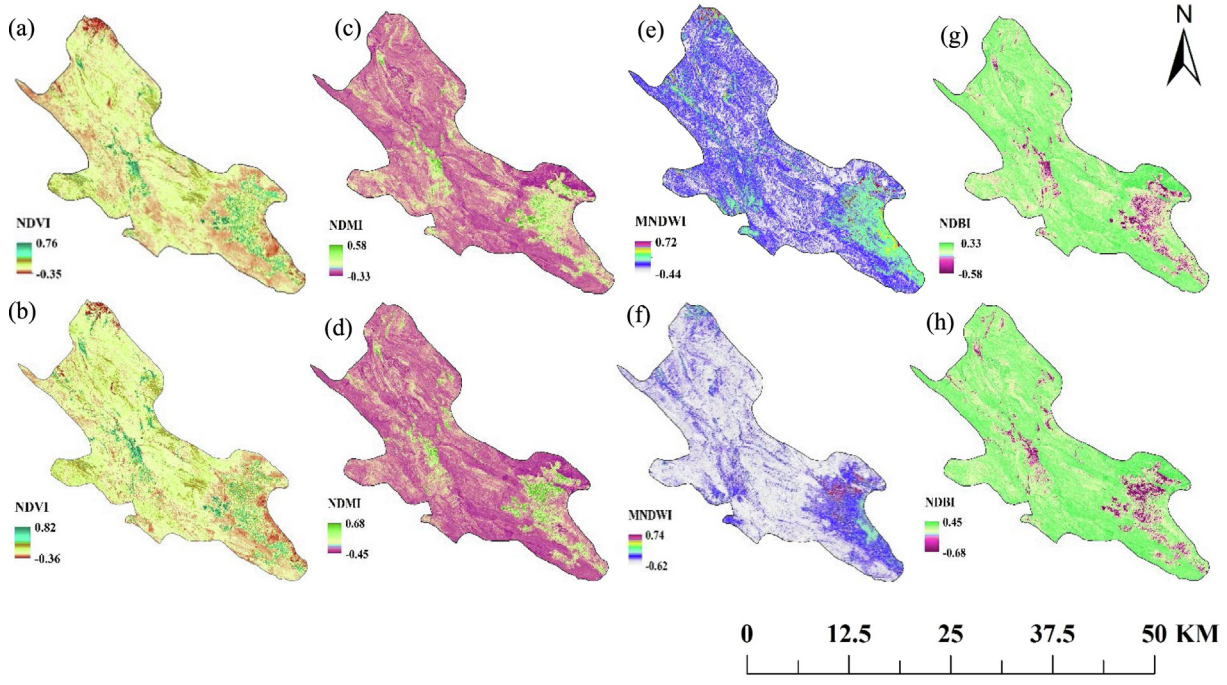

Fig. 7. Map of biophysical indices in the period 1998–2017.

Table 6
Ordinary least-squares (OLS) results for biophisycal, climate and socio-economy factors affecting land surface temperature (LST).

Variable	1998	2017
	R^2	R^2
NDVI	0.95**(−)	0.41*(−)
NDMI	0.66**(−)	0.42**(−)
NDBI	0.403**(+)	0.704**(+)
MNDWI	0.425**(−)	0.729**(−)
Tair	0.15*(+)	0.536**(+)
Solar radiation	0.104*(+)	0.065(+)
FFOCE	0.134*(+)	0.128*(+)
RD	0.12*(+)	0.132*(+)

**, and * represent the significance at 0.01, and 0.05 levels, respectively. (+) and (−) in parentheses indicate that the correlation between the explanatory variable and LST is positive, or negative, respectively.

it ranged from 20 to 54 °C. Fig. 8a shows the NDVI values from 1998 to 2017 in different LST classes. As the number of gardens increased in 2017, the amount of NDVI value generally increased, compared with 1998, in 2017 in all classes except Class 1. The highest and lowest amount of NDVI values for both two periods were seen in zones 1 and 6, respectively.

Fig. 7c and d shows the pattern of NDMI changes for 1998 and 2017. In the study area, NDMI values were within the range of −0.33 to 0.58 for the 1998 period, but they were decreased to −0.45 to 0.68 in 2017. Moreover, LST decreased in both periods with an increase of NDMI. Compared with 1998, LST increased in 2017, rising from 37 to 53 °C in less humid areas, from 33 to 38 °C in semi-humid areas, and from 13 to 22 °C in humid areas. In 2017, the correlation between NDMI and LST was found to be weaker. Furthermore, the R^2 value 0.42, while it was 0.66 in 1998 (Table 6). Fig. 8b shows the NDMI values from 1998 and 2017 in different LST classes. Generally, NDMI decreased in 2017 in all LST classes compared with its values in 1998. The highest value of NDMI was found in class 1 and its lowest value was observed in classes 5 and 6.

Fig. 7e, f shows the spatial distribution of MNDWI for 1998–2017. In the study area, MNDWI values were within the range of −0.44 to 0.72 for the 1998 period with an average of −0.29, but they were decreased to −0.62 to 0.74 in 2017 with the average value of −0.32. Moreover, LST decreased in the 1998–2017 period with an increase of MNDWI. Compared with 1998, LST increased in 2017, with its highest values (>50) found between −0.4 to −0.8 in MNDWI areas. In 2017, the correlation between MNDWI and LST was found to be stronger. Furthermore, the R^2 value was 0.73 in 2017, while it was 0.42 in 1998 (Table 6). Fig. 8c shows the MNDWI values from 1998 to 2017 in different LST classes. Generally, MNDWI decreased in 2017 in all LST classes compared with its values in 1998. The highest value of MNDWI was found in zone 1 and its lowest value was observed in zones 5 and 6.

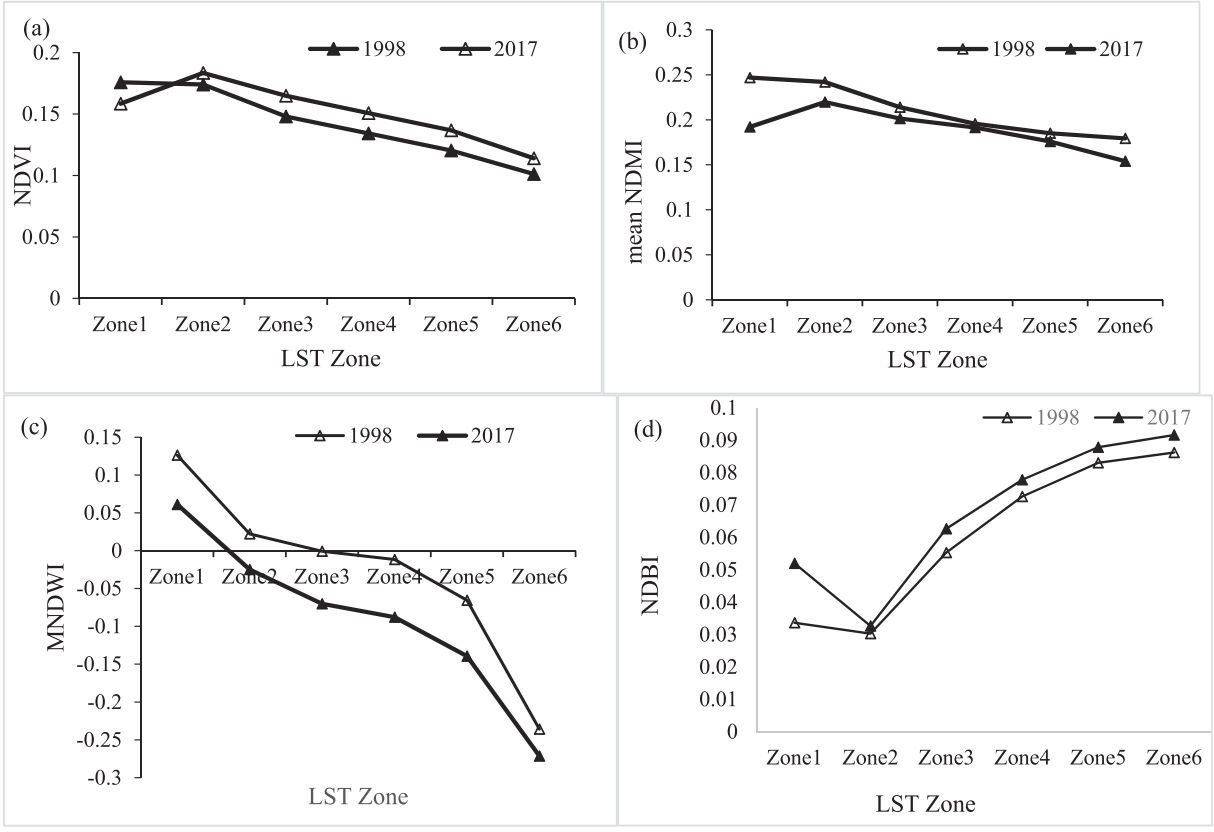

Fig. 8. Variability in the surface biophysical indices at different LST zone (a, b, c and d).

Fig. 7g, h shows the spatial distribution of NDBI. For 1998, the maximum and minimum values of NDBI were −0.58 and −0.33, respectively, while its highest and lowest values were 0.45 and −0.68 in 2017, respectively. In both 1998 and 2017, NDBI increased with an increase in LST. With LST found to be low when NDBI was low, and it was high when the NDBI was high, so positive correlation between LST and NDBI indicating that the growth of residential areas leads to increases in LST. The correlation between NDBI and LST was found to be stronger in 2017. R^2 was 0.7 in this year, while it was 0.42 in 1998 (Table 6). Fig. 8d shows the NDBI values for 1998 and 2017 in different LST classes. Generally, NDBI increased in 2017 in all LST classes compared with its values in 1998. The highest value of NDBI was found in class 6 and its lowest value was observed in classes 1 and 2.

3.2.4. Socio-economic factors

Fig. 9a and b shows the temporal and spatial distribution of FFCOE and its relevant linear regression analysis. Temporally, the total amount of FFCOE was found to have increased from 256 in 1998 to 855 in 2017. Spatially, CO2 has been emitted from the southeast to the southwest, with the NDBI pattern being the same in both years. Moreover, LST and FFCOE were found to have a significant positive correlation, with LST increased in both periods with an increase in FFCOE. Though the coefficient of determination was not high in 1998 and 2017, the results were statistically significant (P0.001).

Fig. 9c, d shows the road density distribution pattern and its relationship with LST. Road density has increased from 8529 km in 1998 to 15590 km in 2017. Compared with 1998, road density increased in 2017 in the western and eastern parts of the region. In both periods, LST increased with an increase in road density, with the correlation of these two factors being higher in 2017 than in 1998. Here, the amount of the coefficient of determination was not high, but the results were statistically significant.

3.2.5. Climate factors

3.2.5.1. Solar radiation. Solar radiation is known as a key effective factor on the temporal and spatial changes of LST at a regional scale. In this study, the elevation range of the region was determined with 100 m distances, and a linear

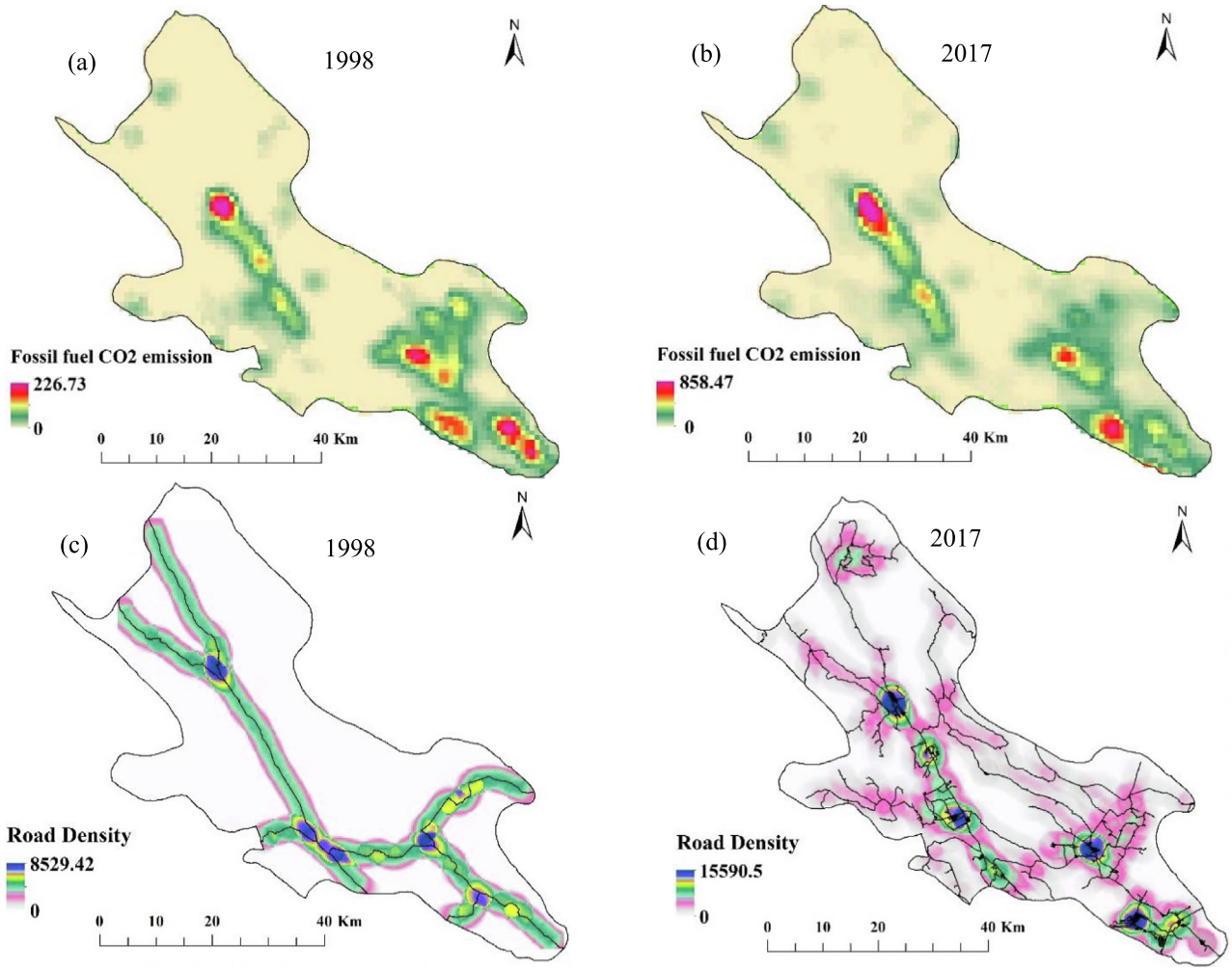

Fig. 9. Maps of ffoce changes (a, b) amd road density for study area.

regression was performed between solar radiation and LST. Fig. 10 shows the results of regression analysis including RMSE, R^2, and the extent of solar radiation changes in each elevation range for 1998 and 2017. Comparing the values found for 1998 and 2017, it could be concluded that the relationship between solar radiation and LST is better in 1998 than in 2017. In 1998 and 2017, the average value of R^2 was found as 0.3 and 0.23, respectively. On the other hand, the regression indicated that RMSE was generally lower in 1998 than in 2017.

Temporal changes of solar radiation at different elevations indicated a decreasing trend with an increase in elevation for 1998 and 2017 (Fig. 10b), being severe at the first four elevation ranges, remaining constant in the middle elevation range, and slowly decreased in the last 7 elevation ranges. Taking the changes in solar radiation with elevation, it could be argued that the sensitivity of LST changes to solar radiation is higher in low elevations than the high ones. The trend of changes in solar radiation with elevation indicates the negligible effect of this factor on LST in the study region. Considering the constant to a low-decreasing trend of changes in most of the elevation classes, it could be said that climate changes along with thermal properties of the surface and vegetation are more effective on LST than solar radiation.

3.2.5.2. Air temperature. In 1998 and 2017, LST increased with the rise of air temperature (Table 6). In 2017, there was a stronger correlation between LST and air temperature at about 0.53, while in 1998 the correlation was found to be 0.15. In high and mountainous regions, the strong relationship between temperature and LST makes measuring these two factors a complicated process. In the study area, the R^2 of the areas with less than 2700 m altitude was more than 0.9 in 2017, but it was less than 0.9 in areas with over 2900 m altitude in the same year (Fig. 11a). In

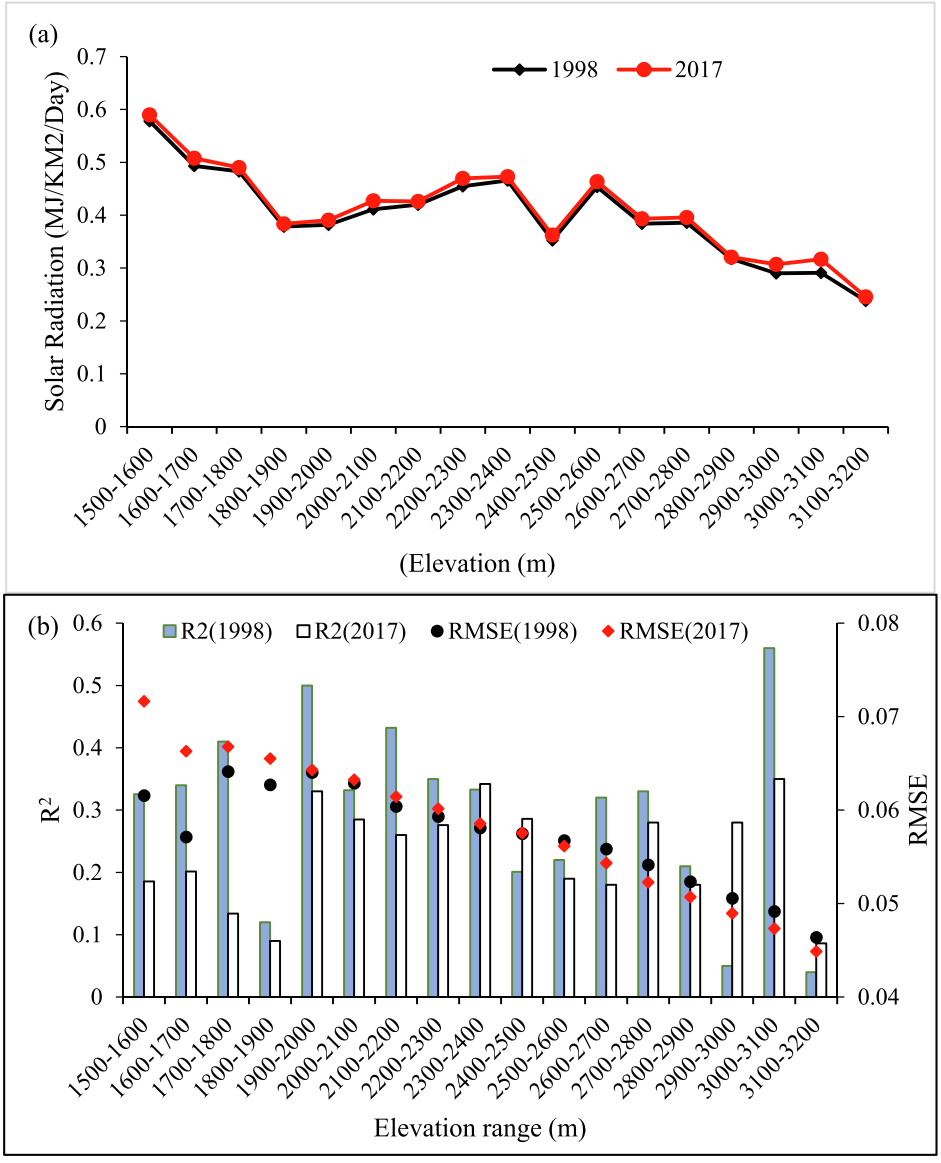

Fig. 10. OLS results between the solar radiation and the LST at different elevation ranges. (a) R^2 and RMSE of study area (b).

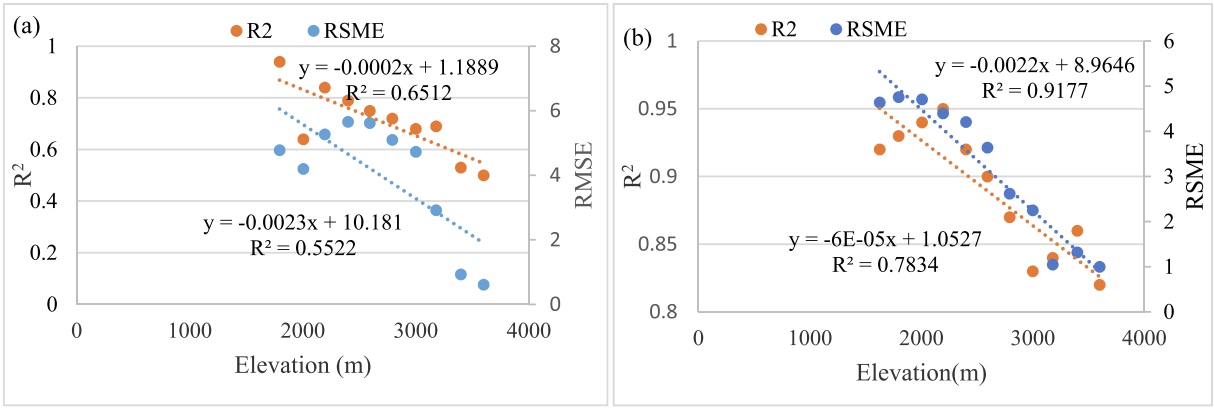

Fig. 11. R^2 and RSME at different elevation ranges in 1998 (a) and 2017 (b).

1998, the R^2 of the areas with less than 2700 m altitude was over 0.7, but it was less than 0.7 in areas with over 2900 m altitude in the same year (Fig. 11b). Furthermore, RSME showed a decreasing trend with the rise in elevation during the study period, and its value was found to be lower in 2017 than in 1998.

3.3. Determining the optimal regression model

In this study, all effective factors on LST at a significance level of 5% were selected for the study period and entered into the best-subset regression. As there were 10 important factors throughout the study period, 10 regression models were created for each period. Fig. 12 shows the results of the subset regression model. Considering the fact that a lower AIC means that a model with fewer variables could show more LST changes thus the lowest amount of AIC was selected as the optimal model. For 1998, five factors including air temperature, MNDWI, NDVI, aspect, and solar radiation with $R^2 = 0.512$ were taken into account, and AIC = 0.76 was selected as the optimal model. For 2017, elevation, NDVI, MNDWI,

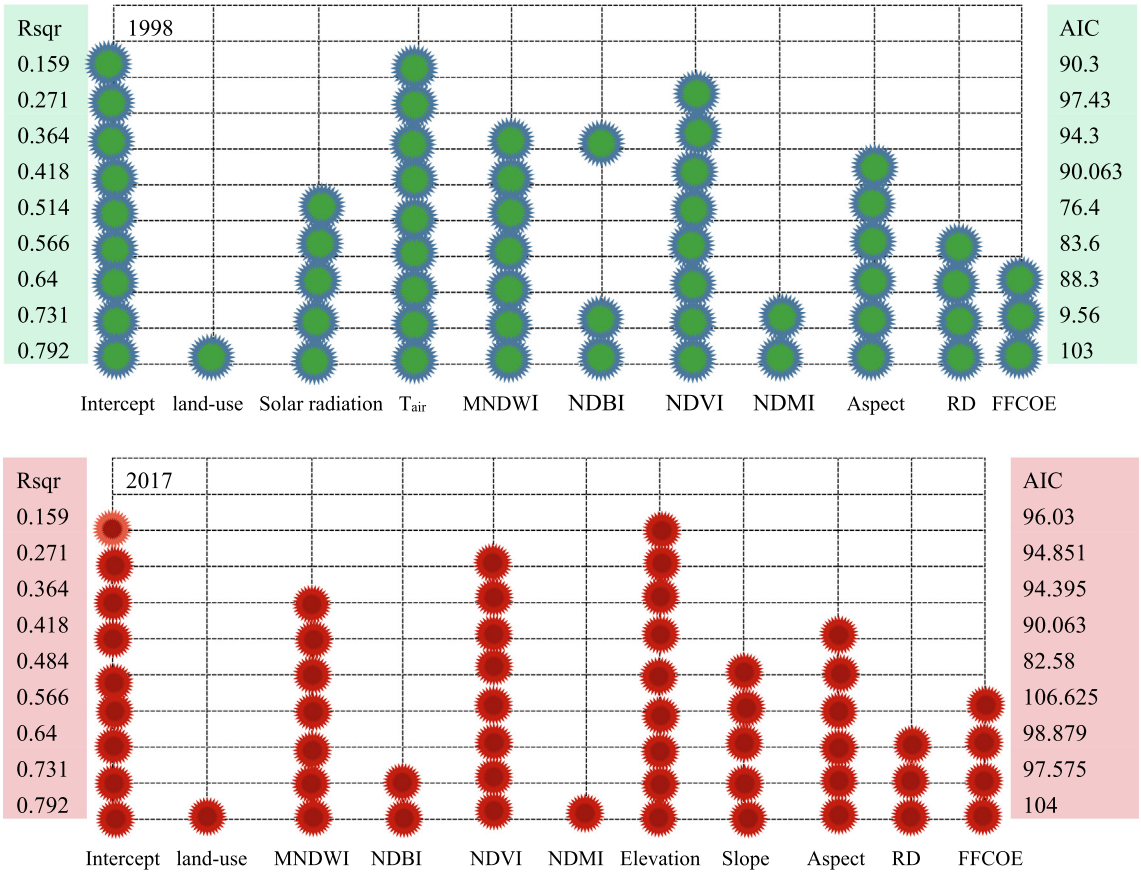

Fig. 12. The results of best- subset regression in the 1998–2017 period.

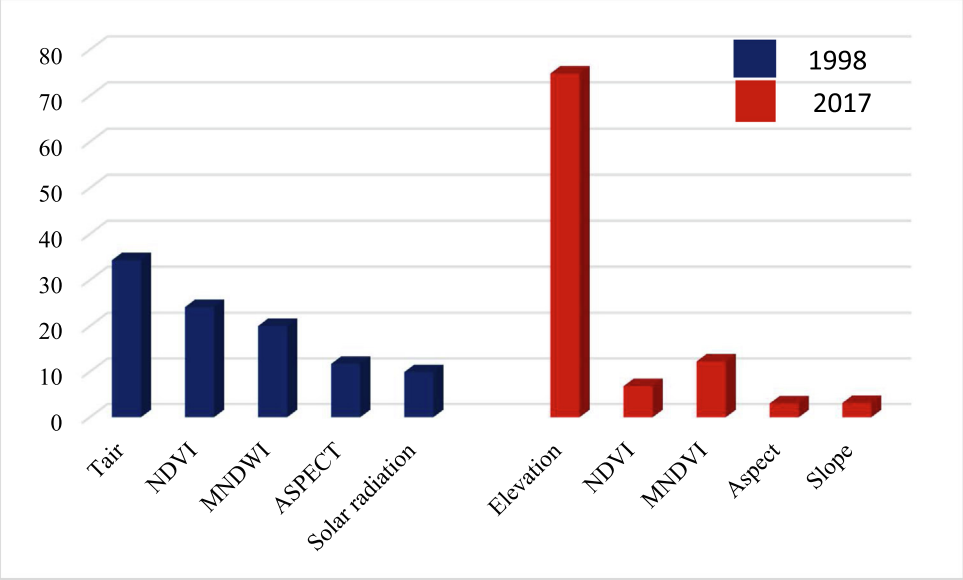

Fig. 13. Determining the relative importance of effective factors on LST via HP Analysis.

aspect, and slope with $R^2 = 486$ and AIC = 82.58 were entered into the optimal model.

3.4. Determining the relative importance of effective factors on LST

To determine the relative importance of effective factors on LST, Hierarchical Partitioning analysis was used. According to the results of this analysis shown in Fig. 13, the air temperature was the most effective factor on LST with 34.27%, while Aspect, MNDWI, NDVI, and solar radiation were 24.12, 20.02, 11.71, and 9.89 percent effective, respectively. In 2017, elevation was the most effective factor in LST changes with 72.82% influence. In this period, Aspect, MNDWI, NDVI, and slope were found to be 6.8, 12.24, 3, and 3.11 percent effective on LST changes.

4. Discussion

In different landscapes, the absorption and emission of heat vary according to different types of land cover. Any change in the landscape, therefore, significantly affect the LST changes. The results of this study showed that the Kappa coefficient was higher than 0.85 for all the images recorded within the study period, proving high accuracy of the classification which is, thus, consistent with the results found by Nurwanda and Honjo (2018).

Moreover, the maximum and minimum values of LST were observed in gardens, barren soil, and residential areas, respectively. As the surface temperature is very sensitive to vegetation and soil moisture, higher-density land uses have lower temperatures (Rhee et al., 2014). Vegetation can reduce the amount of heat stored in the soil and surface structures through transpiration (Babalola and Akinsanola, 2016). Furthermore, the temperature is higher in residential areas and lands with bare soil than in other types of land use. In residential areas, soil, asphalt, and cement heat up and absorb the heat more quickly than other surfaces do. Their impermeability and relatively low thermal inertia also make their temperature to be higher than other kinds of surfaces (Feizizadeh et al., 2013). In barren and shallow soil LST increases due to sparse vegetation, low surface water infiltration, and human intervention (Kayet et al., 2016; Tian et al., 2017).

The results of this study suggested a negative correlation between elevation and LST. The reason behind the decrease of LST with the increase in elevation could be attributed to temperature, as the temperature decreases with an increase in elevation (Peng et al., 2020). The temperature decreases in the troposphere with increasing elevation, as the further we move away from the atmosphere of the earth, the less heated the air would be through the heat reflected from the earth's surface. On the other hand, the density of air and its ability to directly absorb the solar thermal energy decrease with an increase in elevation, making the temperature lower as a result (Zhao et al., 2016). In a similar study, Zhang et al. (2018) found an negative correlation between LST and elevation in the Chinese Ebinur lake basin.

Generally, the results of the current study indicated a decreasing trend of the LST's lapse rate with increasing slope. As precipitation is mostly lost as runoff on steep slopes, there is less infiltrated water and moisture in the soil, making the range of highest and lowest LST values increase which would, in turn, leads to the reduction of surface temperature lapse rate. On the other hand, soil erosion may limit the growth and expansion of vegetation on steep slopes, getting the LST increase subsequently. The results of this study are consistent with those found by He et al. (2019) and Tomaszewskaa and Henebryb (2020) in terms of the decrease in lapse rate with increasing slope.

Results show that the effect of different aspects on LST could be a unique feature for different places in different years. Changes in aspect may result from the differences in solar radiation on the surface. Sunny sided slopes receive more radiation, helping them get warm more quickly than the opposite slopes. In general, the lapse rate is higher on sunny slopes than the shaded ones. Higher values of the surface temperature lapse rate in sunny slopes compared with those of the shaded ones could be justified by taking this fact into consideration that aspect could create unfavorable environmental conditions for the plant growth, as the southern slopes have a higher temperature and evaporation rates because of being more exposed to the sunlight (Fang et al., 2004). Moreover, because of their higher exposure to sunlight and greater evaporation rates, such slopes provide less moisture and nutrients for the plants to grow (Liu et al., 2019a,b).

Biophysical parameters, which are derived from different bands of satellite imagery, are extensively used in the LST research. In the present work, LST showed different responses to biophysical parameters so that an negative correlation was found between NDVI and LST. Furthermore, in zone 1, NDVI was higher due to the increase in irrigated agriculture and the decrease of residential areas in comparison with the year 2017. The lowest amount of NDVI values for both two periods were seen in zone 6. Compared to other LST zones, residential areas, bare soil, and rain-fed lands increased in 1998 in zone 6, while in 2017 residential areas and poor pastures increased and garden land decreased in this zone, resulting in its lower NDVI and less vegetation than other zones. In addition to controlling the surface temperature through balancing the energy, vegetation affects bare soil and observable land cover. On the other hand, radiative temperature between soil and canopy significantly affects LST (Sandholt et al., 2002; He et al., 2019). Moreover, vegetation influences the thermal properties of the surface. Similarly, in their study to investigate the relationship between NDVI and LST in Chhattisgarh state in India, Guha and Govil1 (2020) found an negative correlation between the two indices. Also, Das and Angadi (2020) asserted the significance of vegetation for LST, showing a negative trend in the correlation between NDVI and LST.

In the current study, NDMI was found to have decreased in 2017 compared with 1998. Moreover, the LST value was low in areas with a higher level of moisture, proving the negative correlation between LST and NDMI. Soil surface moisture depends on the amount of incoming rainfall and outgoing current, vegetation conditions, and soil development. As a considerable amount of water could be stored in vegetation, the plant's body, and the soil, vegetation extent and conditions are regarded as significantly effective factors on LST. Therefore, with the loss of soil and vegetation, the ability to maintain surface moisture decreases, making the LST increases as a result (Brom et al., 2012). In a similar study, Lu et al. (2009) reported that the decrease in humidity led to slow transpiration and consequently an increase in LST, which could be the reason for the negative correlation between NDMI and LST. Zheng et al. (2019) also showed an negative correlation between LST and NDMI.

The results of the correlation between surface temperature and NDBI suggest a positive correlation between these two variables, indicating that the growth of residential areas leads to increases in LST. The results of the current study are consistent with those found by Guo et al. (2015) and Chen and Zhang (2017) who showed a positive correlation between LST and NDBI in their studies. The high temperature in urban environments could be attributed to the presence of hard and impermeable surfaces including concrete surfaces, streets, and bricks that are widely used in such areas (Yuan and Bauer, 2007).

In this study, it was found that MNDWI which represents water areas such as rivers and lakes had decreased in 2017 compared with its rate in 1998. Moreover, the lowest value of MNDWI was observed in zone 6 where the LST value was at its highest rate, which could be attributed to the reduction of water levels in rives, as Khan et al. (2019) reported that water bodies have declined in most parts of the world. The results of our study indicated an negative correlation between LST and MNDWI. As water bodies have a cooling effect on their surroundings, their protection plays a very significant role in adjusting LST; a fact that has been confirmed by a vast majority of relevant studies (Ferreira and Duarte, 2019; Liu et al., 2019a, b; Gogoi et al., 2019; Muro et al., 2018). It could, therefore, be argued that the authorities need to pay more attention to the protection and support of wetlands, lakes, rivers, and other bodies of water (Tan et al., 2020).

GDP is considered as one of the effective factors on socio-economic activities (Ranagalage et al., 2017) which in turn affect the LST in terms of population density, energy demands, and air pollution (Min et al., 2018). Fossil fuel could be regarded as an influential factor in the industry, transportation, electricity generation, and domestic sectors. With increasing GDP, the demand for fossil fuel would be greater in the industry. Increasing CO2 emissions as a result of fossil fuel combustion causes adverse environmental consequences including the rise in temperature (Aderogba, 2011; Agarana et al., 2017). In this study, LST was found to have a positive correlation with FFCOE, indicating the effect of CO2 on LST in the Sepidan region. Moreover, from the spatial point of view, the CO2 emission pattern from the southeast to the southwest was similar to the NDBI pattern. It could, therefore, be argued that the expansion of urban areas via human activities plays an important role in increasing CO2 emission.

Compared to its rate in 1998, road density increased, on the other hand, in 2017 in the Sepidan region. Roads have various ecological effects on plants and their surroundings. In this study, road density increased with increasing LST, proving a positive correlation between these two factors. As the impermeable surfaces such as asphalts increase with the rising number of roads, much rainwater is lost as runoff

and the LST increases consequently (Ragab et al., 2003). On the other hand, regional vegetation is destroyed for the roads to be constructed, and the LST increases with the loss of vegetation (Karim and Mallik, 2008). Moreover, the amount of CO2 emitted from car fossil fuels increases with the rise of road density which in turn considerably affects the LST (Johnston and Johnston, 2004).

In the study area, LST was found to have increased with the rise of air temperature during the 1998–2017 period, indicating a positive correlation between these two factors. The surface of the earth mainly heats up via thermal radiation transmitted from solar insolation (Vancutsem et al., 2010; Benali et al., 2012). With increasing temperature, dry climate, pure solar radiation and evaporation increase, and the degree of cloudiness, soil moisture, atmospheric humidity, and evapotranspiration decrease, making the LST value increase altogether, especially in areas with bare soil ((Donat et al., 2014; El Kenawy et al., 2016). Moreover, the results of this study indicated that with the rising elevation in both two study periods, the RSME between air temperature and LST was of a decreasing trend which is consistent with the results found by Mutiibwa et al. (2015) in terms of the effect of elevation on LST and the decreasing trend of RSME with elevation. The solar radiation is affected by cloudy weather so that in places with less cloudiness, the amount of radiation is more, and therefore the air temperature increases and then LST increases (Zhou et al., 2018).

5. Conclusion

The properties of different surfaces such as water, soil, vegetation, urban covers, etc. affect the changes of atmospheric elements adjacent to the surface, being able to create different thermal patterns at different levels. Rising surface temperatures cause chemical processes that accelerate the formation of ozone molecules and pose a serious threat to human health. Therefore, temporal and spatial changes in LST and the factors affecting it (12 factors) in the Sepidan region during the 1998–2017 period were investigated in the current study. The correlation between LST changes and various topographic, echo-hydrological, and socio-economic factors was examined, using OLS regression, Best-Subset, and hierarchical clustering analysis. The results suggested that LST was significantly affected in a complex way by terrestrial factors. The results of linear regression showed that there was a relationship between topographic factors, vegetation, soil moisture, waterbody, air temperature, solar radiation, and socio-economic factors (road density and fossil fuel), based on which 9 models were created according to 10 factors (out of the those mentioned) with the greatest effects in each period.

For 1998, air temperature and vegetation were identified as the most effective factors on LST, while in 2017 it was the elevation which was found to have the greatest role in LST changes, being 72.82% effective in this regard alone. Considering the above-mentioned facts and the mountainous nature of the region, it could be argued that mostly topographic and climatic factors determine LST changes and that other factors such as water body, socio-economic variables, and land use are less effective in that regard. As in this study, the lowest and highest LST values were found in gardens and residential areas, respectively, it is suggested that deforestation and the conversion of postures into agricultural lands be prevented via appropriate management methods and that artificial forests be created through tree plantation projects. Although this study investigated the effect of 12 different factors on LST, such factors as wind speed, cloud cover, population density, and other possible factors were not taken into account; it is, therefore, recommended that future studies on this topic consider more factors so that the results get improved. Considering the significance of LST for mountainous regions, the findings of this study could be helpful in most of the areas regarding urban affairs, transportation, tourism, and water resources as well as watershed management.

Declaration of Competing Interest

The authors declare that they have no known competing financial interests or personal relationships that could have appeared to influence the work reported in this paper.

References

Aderogba, K.A., 2011. Greenhouse gas emissions and sustainability in Lagos Metropolis, Nigeria. Int. J. Learn. Dev. 1, 46–61.

Agarana, M.C., Bishop, S.A., Agboola, O.O., 2017. Minimizing carbon emissions from transportation projects in Sub-saharan Africa cities using mathematical model: A Focus on Lagos, Nigeria. Procedia Manuf. 7, 596–601.

Aguilar, C., Herrero, L., Polo, M.J., 2010. Topographic Effects on Solar Radiation Distribution in Mountainous Watersheds and Their Influence on Evapotranspiration Estimates at Watershed Scale. Hydrol. Earth Syst. Sci. 14 (12), 2479–2494.

Alemu, M.M., 2019. Analysis of spatio-temporal land surface temperature and normalized difference vegetation index changes in the Andassa watershed, Blue Nile Basin, Ethiopia. J. Resourc. Ecol. 10 (1), 77–86.

Amiri, R., Weng, Q., Alimohammadi, A., Alavipanah, S.K., 2009. Spatial–Temporal Dynamics of Land SurfaceTemperature in Relation to Fractional Vegetation Cover and Land Use/Cover in the Tabriz Urban Area, Iran. Remote Sens. Environ. 113 (12), 2606–2617.

Anthony, Y., Kuk, C., 1984. All subsets regression in a proportional hazards model. Biometrika 71 (3), 587–592.

Ayansina, A., 2016. Seasonality in the daytime and night-time intensity of land surface temperature in a tropical city area. Sci. Total Environ. 557, 415–424.

Babalola, O., Akinsanola, A., 2016. Change detection in land surface temperature and land use /land cover over Lagos Metropoli, Nigeria. J. Remote Sens. & GIS 5 (2), 1–7.

Benali, A., Carvalho, A.C., Nunes, J.P., Carvalhais, N., Santos, A., 2012. Estimating air surface temperature in Portugal using MODIS LST data. Remote Sens. Environ. 124, 108–121.

Berg, A., Lintner, B.R., Findell, K.L., Malyshev, S., Loikith, P.C., Gentine, P., 2014. Impact of Soil Moisture-Atmosphere Interactions on Surface Temperature Distribution. J. Climate. 27 (21), 7976–7993.

Broma, J., Nedbal, V., Prochazkaa, J., Pecharova, E., 2012. Changes in vegetation cover, moisture properties and surface temperature of a

brown coal dump from 1984 to 2009 using satellite data analysis. Ecol. Eng.. 43, 45–52.
Chang, Y., Ding, Y., Zhao, Q., Zhang, S., 2017. Remote Estimation of Terrestrial Evapotranspiration by Landsat 5 TM and the SEBAL Model in Cold and High-Altitude Regions: A Case Study of the Upper Reach of the Shule River Basin, China. Hydrol. Processe. 31 (3), 514–524.
Chen, X., Zhang, Y., 2017. Impacts of urban surface characteristics on spatiotemporal pattern of land surface temperature in Kunming of China. Sustainable Cities Soc. 32, 87–99.
Clinton, N., Gong, P., 2013. MODIS detected surface urban heat islands and sinks: global locations and controls. Remote Sens. Environ. 134, 294–304.
Das, S., Angadi, D.P., 2020. Land use-land cover (LULC) transformation and its relation with land surface temperature changes: A case study of Barrackpore Subdivision, West Bengal, India. Remote Sens. Appl.: Soc. Environ. 20, 100322.
Dissanayake, D., Morimoto, T., Murayama, Y., Ranagalage, M., Handayani, H.H., 2019. Impact of Urban Surface Characteristics and Socio-Economic Variables on the Spatial Variation of Land Surface Temperature in Lagos City, Nigeri. Sustainability. 11, 25.
Donat, M.G., Peterson, T.C., Brunet, M., King, A.D., Almazroui, M., Kolli, R.K., Boucherf, D., Al-Mulla, A.Y., Nour, A.Y., Aly, A.A., 2014. Changes in extreme temperature and precipitation in the Arab region: Long-term trends and variability related to ENSO and NAO. Int. J. Climatol. 34, 581–592.
El Kenawy, A.M., McCabe, M.F., Vicente-Serrano, S.M., Robaa, S.M., Lopez-Moreno, J.I., 2016. Recent changes in continentality and aridity conditions over the Middle East and North Africa region, and their association with circulation patterns. Clim. Res. 69, 25–43.
Eludoyin, O.M., Adelekan, I.O., Webster, R., Eludoyin, A.O., 2013. Air temperature, relative humidity, climate regionalization and thermal comfort of Nigeria. Int. J. Climatol. 34 (6), 2000–2018.
Esfandyari Bayat, M.J., Rameh, H., 2016. Biostratigraphy of the Gurpi Formation in Sepidan section, Interior Fars basin based on planktonic foraminifera. Geopersia. 6 (2), 211–221.
Estoque, R.C., Murayama, Y., Myint, S.W., 2017. Effects of landscape composition and pattern on land surface temperature: an urban heat island study in the megacities of Southeast Asia. Sci. Total Environ. 577, 359–359.
Fang, J., Shen, Z., Cui, H., 2004. Ecological characteristics of mountains and research issues of mountain ecology. Biodiversity. 12 (1), 10–19.
Feizizadeh, B., Blaschke, T., Nazmfar, H., Akbari, E., Kohbanani, H.R., 2013. Monitoring land surface temperature relationship to land use/land cover from satellite imagery in Maraqeh County, Iran. J. Environ. Plann. Manage. 56 (9), 1290–1315.
Ferreira, L.S., Duarte, D.H.S., 2019. Exploring the relationship between urban form, land surface temperature and vegetation indices in a subtropical megacity. Urban Climate. 27, 105–123.
Ghosh, M.K., Kumar, L., Roy, C., 2015. Monitoring the coastline change of Hatiya Island in Bangladesh using remote sensing techniques. ISPRS J. Photogramm. Remote Sens. 101 (1), 137–144.
Gluch, R., Quattrochi, D.A., Luvall, J.C., 2006. A multi-scale approach to urban thermal analysis. Remote Sens. Environ. 104, 123–132.
Gogoi, P.P., Vinoj, V., Swain, D., Roberts, G., Dash, J., Tripathy, S., 2019. Land use and land cover change effect on surface temperature over Eastern India. Sci Rep. 9, 8859.
Guha, S., Govil, H., 2020. An assessment on the relationship between land surface temperature and normalized difference vegetation index. Environ. Develop. Sustainab. 7 (22).
Guo, G., Wu, Z., Xiao, R., Chen, Y., Liu, X., Zhang, X., 2015. Impacts of urban biophysical composition on land surface temperature in urban heat island clusters. Landsc. Urban Plan. 135, 1–10.
He, J., Zhao, W., Li, A., Wen, F., Yu, D., 2018. The impact of the terrain effect on land surface temperature variation based on Landsat-8 observations in mountainous areas. Int. J. Remote Sens. 40 (6), 1808–1827.
Holzman, M.E., Rivas, R., Piccolo, M.C., 2014. Estimating Soil Moisture and the Relationship with Crop Yield Using Surface Temperature and Vegetation Index. Int. J. Appl. Earth Obser. Geoinformat. 28, 181–192.
Huang, X.M., Schneider, A., Friedl, M.A., 2016. Mapping sub-pixel urban expansion in China using MODIS and DMSP/OLS nighttime lights. Remote Sens. Environ. 175, 92–108.
Ibrahim, M., Abu-Mallouh, H., 2018. Estimate land surface temperature in relation to land use types and geological formations using spectral remote sensing data in northeast Jordan. Open J. Geol. 8 (02), 174–185.
Ivanov, V.Y., Bras, R.L., Vivoni, E.R., 2008. Vegetation-Hydrology Dynamics in Complex Terrain of Semiarid Areas: A Mechanistic Approach to Modeling Dynamic Feedbacks. Water Resourc. Res. 44 (3), 44–58.
Jin, M., Dickinson, R., 2010. Land surface skin temperature climatology: Benefitting from the strengths of satellite observations. Environ. Res. Lett. 5 (4), 044004.
Jin, X.M., Wan, L., Zhang, Y.K., Hu, G., Echaepman, M.E., Clevers, J. G.P.W., 2009. Quantification of spatial distribution of vegetation in the Qilian Mountain area with MODIS NDVI. Int. J. Remote Sens. 30 (21), 5751–5766.
Johnston, F.M., Johnston, S.W., 2004. Impacts of road disturbance on soil properties and on exotic plant Occurrence in subalpine areas of the Australian Alps. Arctic, Antarctic, Alpine Res. 36 (2), 201–207.
Karim, M.N., Mallik, A.U., 2008. Roadside revegetation by native plants. Ecol. Eng. 32, 222–237.
Kayet, N., Pathak, K., Chakrabarty, A., Sahoo, S., 2016. Spatial impact of land use/land cover change on surface temperature distribution in Saranda Forest, Jharkhand. Model. Earth Syst. Environ. 2 (3), 127–139.
Khan, N., Shahid, S., Chung, E.S., Kim, S., Ali, R., 2019. Influence of Surface Water Bodies on the Land Surface Temperature of Bangladesh. Sustainability 11, 6754.
Kikon, N., Singh, P., Singh, S.K., Vyas, A., 2016. Assessment of urban heat islands (UHI) of Noida City, India using multi-temporal satellite data. Sustain. Cities So. 22, 19–28.
Kotharkar, R., Surawar, M., 2016. Land use, land cover, and population density impact on the formation of canopy urban heat islands through traverse survey in the Nagpur urban area, India. J. Urban Plann. Dev. 142 (1).
Krall, J.M., Uthoff, V.A., Harley, J.B., 1975. A step-up procedure for selecting variables associated with survival. Biometrics. 31 (1), 49–57.
Li, X.M., Zhou, W.Q., Ouyang, Z.Y., 2013a. Relationship between land surface temperature and spatial pattern of greenspace: what are the effects of spatial resolution? Landsc. Urban Plan. 114, 1–8.
Li, Z., Jia, L., Jing, L., 2014. On Uncertainties of the Priestley-Taylor/LST-Fc Feature Space Method to Estimate Evapotranspiration: Case Study in an Arid/Semiarid Region in Northwest China. Remote Sensing. 7 (1), 447–466.
Liu, L., Zhang, L., 2011. Urban Heat Island Analysis Using the Landsat TM Data and ASTER Data: A Case Study in Hong Kong. Remote Sensing 3, 1535–1552.
Liu, M., Che, Y., Jiao, J., Li, L., Jiang, X., 2019a. Exploring the community phylogenetic structure along the slope aspect of subalpine meadows in the eastern Qinghai-Tibetan Plateau, China. Ecol. Evol. 9, 5270–5280.
Liu, T., Yu, L., Zhang, S., 2019b. Land Surface Temperature Response to Irrigated Paddy Field Expansion: a Case Study of Semi-arid Western Jilin Province, China. Sci Rep 9, 5278.
Lu, D.S., Li, G.Y., Moran, E., Hetrick, S., 2013. Spatiotemporal analysis of land-use and land-cover change in the Brazilian Amazon. Int. J. Remote Sens. 34 (16), 5953–5978.
Lu, Y., Feng, X., Xiao, P., Sheng, C., 2009. Urban heat island in summer of Nanjing based on TM data. Conference Urban Remote Sensing Event. 1.
Mac, N.R., 2000. Regression and model-building in conservation biology, biogeography and ecology: the distinction between and reconciliation of predictive and explanatory models. Biodivers. Conserv. 9 (5), 655–671.

McCutchan, M.H., Fox, D.D., 1986. Effect of Elevation and Aspect on Wind, Temperature and Humidity. J. Climate Appl. Meteorol. 25 (12), 1996–2013.

Meng, Q., Zhang, L., Sun, Z., Meng, F., Wang, L., Sun, Y., 2018. Characterizing spatial and temporal trends of surface urban heat island effect in an urban main builtup area: a 12-year case study in Beijing, China. Remote Sens. Environ. 204, 826–837.

Mihalcea, C., Brock, B.W., Diolaiuti, G., Agata, C.D., Citterio, M., Kirkbride, M.P., Culter, M.E.J., Smiraglia, C., 2008. Using ASTER satellite and ground-based surface temperature measurements to derive supraglacial debris cover and thickness patterns on Miage Glacier (Mont Blanc Massif, Italy). J. Cold Regions Sci. Technol. 52, 341–354.

Min, M., Zhao, H., Miao, C., 2018. Spatio-temporal evolution analysis of the urban heat island: A case study of Zhengzhou City, China. Sustainability. 10, 1992.

Minder, J.R., Mote, P.W., Lundquist, J.D., 2010. Surface Temperature Lapse Rates over Complex Terrain: Lessons from the Cascade Mountains. J. Geophys. Res.: Atmosph. 115 (D14), 1–13.

Muro, J., Strauch, A., Heineman, S., Steinbach, S., Thonfeld, F., Waske, B., Diekkrüger, B., 2018. Land surface temperature trends as indicator of land use changes in wetlands. Int. J. Appl. Earth Obser. Geoinformat. 70, 62–71.

Mutiibwa, D., Strachan, S., Albright, T., 2015. Land surface temperature and surface air temperature in complex terrain. IEEE J. Sel. Top. Appl. Earth Obser. Remote Sens. 8 (10), 4762–4774.

Neteler, M., 2010. Estimating daily land surface temperatures in mountainous environments by reconstructed MODIS LST data. Remote Sensing. 2, 333–351.

Nurwanda, A., Honjo, T., 2018. Analysis of land use change and expansion of surface urban heat island in Bogor city by remote sensing. ISPRS Int. J. Geo-Informat. 7 (5), 165–178.

Peng, J., Ma, J., Liu, Q.Y., Liu, Y.X., Li, Y.R., Yue, Y.Y., 2018. Spatial-temporal change ofland surface temperature across 285 cities in China: an urban-rural contrast perspective. Sci. Total Environ. 635, 487–497.

Peng, S.S., Piao, S.L., Ciais, P., Friedlingstein, P., Ottle, C., Bréon, F.M., Nan, H.J., Zhou, L.M., Myneni, R.B., 2012. Surface urban heat island across 419 global big cities. Environ. Sci. Technol. 46 (2), 696–703.

Peng, W., Zhou, J., Wen, L., Xue, S., Dong, L., 2017. Land surface temperature and its impact factors in Western Sichuan Plateau, China. Geocarto Int. 32 (8), 919–934.

Peng, X., Wu, W., Zheng, Y., Sun, J., Hu, T., Wang, P., 2020. Correlation analysis of land surface temperature and topographic elements in Hangzhou, China. Sci. Rep. 10, 10451.

Ragab, R., Rosier, P., Dixon, A., Bromley, J., Cooper, J., 2003. Experimental study of water fluxes in a residential area: Road infiltration, runoff and evaporation. Hydrolog. Processes. 17 (12), 2423–2437.

Ranagalage, M., Estoque, R.C., Murayama, Y., 2017. An urban heat island study of the Colombo Metropolitan Area, Sri Lanka, based on Landsat Data (1997–2017). ISPRS Int. J. Geo-Inf. 6, 189.

Rhee, J., Park, S., Lu, Z., 2014. Relationship between land cover patterns and surface temperature in urban areas. GISci. Remote Sens. 51, 521.

Rouse, J.W., Haas, H., Schell, J.A., Deering, D.W., 1974. Monitoring vegetation system in the great plains with ERTS. In: Proceedings of the Third Earth Resources Technology Satellite-1 Symposium, Greenbelt, USA; NASA SP-351. pp. 3010–3017.

Sandholt, I., Rasmussen, K., Andersen, J., 2002. A Simple Interpretation of the Surface Temperature/Vegetation Index Space for Assessment of Surface Moisture Status. Remote Sens. Environ. 79 (2–3), 213–224.

Sattari, F., Hashim, M., Pour, A.B., 2018. Thermal sharpening of land surface temperature maps based on the impervious surface index with the TsHARP method to ASTER satellite data: a case study from the metropolitan Kuala Lumpur, Malaysia. Measurement., 125262–125278

Shi, P., Qin, Y., Liu, Q., 2019. Soil respiration and response of carbon source changes to vegetation restoration in the Loess Plateau, China. Sci. Total Environ. 707, 135505.

Sobrino, J.A., Li, Z.L., Stoll, M.P., Becker, F., 1996. Multi-channel and multi-angle algorithms for estimating sea and land surface temperature with ATSR data. Int. J. Remote Sens. 17, 2089–2114.

Sobrino, J.A., Jimenez-Munoz, J.C., Paolini, L., 2004. Land surface temperature retrieval from LANDSAT TM 5. Remote Sens. Environ. 90 (4), 434–440.

Sobrino, J.A., Jime´nez-Muñoz, J.C., Soria, G., Ruescas, A.B., Danne, O., Brockmann, C., Ghent, D., Remedios, J., North, P., Merchant, C., 2016. Synergistic use of MERIS and AATSR as a proxy for estimating Land Surface Temperature from Sentinel-3 data. Remote Sens. Environ. 179, 149–161.

Steinacker, R., Ratheiser, M., Bica, B., Chimani, B., Dorninger, M., Gepp, W., Lotteraner, C., Schneider, S., Tschannett, S., 2006. A mesoscale data analysis and downscaling method over complex terrain. Monthly Weather Rev. 134, 2758–2771.

Tan, J., Yu, D., Li, Q., Tan, X., Zhou, W., 2020. Spatial relationship between land-use/land-cover change and land surface temperature in the Dongting Lake area, China. Sci. Rep. 10, 9245.

Tian, Y., Bai, X., Wang, S., Qin, L., Li, Y., 2017. Spatial-temporal changes of vegetation cover in Guizhou Province, Southern China. Chinese Geograph. Sci. 27 (1), 25–38.

Tomaszewskaa, M.A., Henebryb, G.M., 2020. How much variation in land surface phenology can climate oscillation modes explain at the scale of mountain pastures in Kyrgyzstan. Int. J. Appl. Earth Obs. Geoinformat. 87, 102053.

Tomlinson, C.J., Chapman, L., Thornes, J.E., Baker, C., 2011. Remote Sensing Land Surface Temperature for Meteorology and Climatology: A Review. Meteorol. Appl.. 18 (3), 296–306.

Vancutsem, C., Ceccato, P., Dinku, T., Connor, S.J., 2010. Evaluation of MODIS land surface temperature data to estimate air temperature in di_erent ecosystems over Africa. Remote Sens. Environ. 114, 449–465.

Van De Kerchove, R., Lhermitte, S., Veraverbeke, S., Goossens, R., 2013. Spatio-Temporal Variability in Remotely Sensed Land Surface Temperature, and Its Relationship with Physiographic Variables in the Russian Altay Mountains. Int. J. Appl. Earth Obser. Geoinformat. 20, 4–19.

Valor, E., Caselles, V., 2005. Validation of the vegetation cover method for land surface emissivity estimation. In: Recent Research Developments in Thermal Remote Sensing; Research Singpost: Kerala, India, pp. 1–20.

Xu, H., 2005. A study on information extraction ofwater body with the modified normalized difference water index (MNDWI). J. Remote Sen. 9, 589–595.

Xu, T., Bateni, S.M., Margulis, S.A., Song, L., Liu, S., Ziwei, X., 2016. Partitioning Evapotranspiration into Soil Evaporation and Canopy Transpiration via a Two-Source Variational Data Assimilation System. J. Hydrometeorol. 17 (9), 2353–2370.

Yao, R., Wang, L., Huang, X., Niu, Y., Chen, Y., Niu, Z., 2018. The influence of different data and method on estimating the surface urban heat island intensity. Ecol. Indicat. 89, 45–55.

Yuan, F., Bauer, M.E., 2007. Comparison of impervious surface area and normalized difference vegetation index as indicators of surface urban heat island effects in Landsat imagery. Remote Sens. Environ. 106 (3), 375–386.

Yue, W., Liu, X., Zhou, Y., Liu, Y., 2019. Impacts of urban configuration on urban heat island: an empirical study in China mega-cities. Sci. Total Environ. 671, 1036–1046.

Zhang, F., Kung, H., Johnson, V.C., LaGrone, B., Wang, J., 2018. Change Detection of Land Surface Temperature (LST) and some Related Parameters Using Landsat Image: a Case Study of the Ebinur Lake Watershed Xinjiang, China. Wetland. 38, 65–80.

Zhao, W., Li, A.N., Zheng, J., 2016. A study on land surface temperature terrain effect over mountainous area based on Landsat 8 thermal infrared data. Remote Sens. Technol. Appl. 31 (1), 63–73.

Li, Z.L., Tang, B.H., Hua, W., Ren, H., Yan, G., Wan, Z., Trigo, I.F., Sobrino, J.A., 2013b. Satellite-Derived Land Surface Temperature: Current Status and Perspectives. Remote Sensing Environ. 131, 14–37.

Zheng, H., Chen, C.H., Pan, W., Cai, Y., Chen, Z., 2019. Impact of Land Use/Land Cover Changes on the Thermal Environment in Urbanization: A Case Study of the Natural Wetlands Distribution Area in Minjiang River Estuary, China. Pol. J. Environ. Stud. 28 (4), 3025–3041.

Zhou, D., Xiao, J., Bonafoni, S., Berger, C., Deilami, K., Zhou, Y., Frolking, S., Yao, R., Qiao, Z., Sobrino, J., 2018a. Satellite remote sensing of surface urban heat islands: progress, challenges, and perspectives. Rem. Sens. 11, 48.

Zhou, J., Chen, Y., Zhang, X., Zhan, W., 2013. Modelling the Diurnal Variations of Urban Heat Islands with Multi-Source Satellite Data. Int. J. Remote Sens. 34 (21), 7568–7588.

Zhou, Z., Wang, L., Lin, A., Zhang, M., Niu, Z., 2018b. Innovative trend analysis of solar radiation in China during 1962–2015. Renewable Energy 119, 675–689.